Metallography, Microstructure, and Analysis (2022) 11:415–424
https://doi.org/10.1007/s13632-022-00855-w

PEER REVIEWED

Comparative Study of Microstructure and Properties of Hypoeutectic Al-Si Alloys Being Cast With and Without Melt Thermal Treatment

Sunil Manani[1] · Aashendra Patodi[1] · Mrigesh Navalkishor Verma[1] · Ajaya Kumar Pradhan[1]

Received: 1 February 2022 / Revised: 30 April 2022 / Accepted: 10 May 2022 / Published online: 27 May 2022

Abstract

This study investigated the microstructure and mechanical properties of several hypoeutectic Al-xSi (x = 0, 1, 3, 5, 7, 9) alloys prepared with and without melt thermal treatment. The overall study showed a trend of effective utilization of grain refiner until the transition point (3 wt.% Si) and the slope of graph between grain size vs. wt.% of Si remain similar for the samples prepared with or without chemical refinement. This also indicates that the role of Si in decreasing grain size is more dominating than the poisoning of Ti above transition point. Melt thermal-treated alloys exhibited less significant changes in grain size, especially below the transition point, but significant changes in their mechanical properties. The melt thermal treatment also causes partial refinement of eutectic Si particles by which the coarse silicon particles are broken up into smaller pieces and this has neither been observed in unrefined alloys nor refined alloys.

Keywords Hypoeutectic Al-xSi alloy · Melt thermal treatment · Grain refiner · Grain size · Transition point

Introduction

The hypoeutectic Al-Si alloys are widely used in the automotive and structural fields by virtue of their advantages such as ease of casting, compatible or superior corrosion resistance to other usually used alloys, good weldability, and sufficiently good strength [1–5]. However, these alloys in cast condition consist of coarse α-Al dendrites and acicular Si phase, which leads to poor mechanical properties. For improved mechanical properties, alloys should have refined primary α-Al grains and shape modified eutectic Si phase [6–8]. In recent years, grain refiners like Al-Ti, Al-B, and mischmetal (MM) such as Ce- and Nb-based master alloys have refined Al-Si alloys microstructure [9–15]. Each of these refiners has its drawbacks, which the current industries are dealing with. For example, Ti-based refiners exhibit a poisoning problem with Si, especially in melt with Si content higher than 3.5 wt.% [16–18]. This ultimately affects the grain refining efficiency of those refiners negatively. In other words, Ti-based refiners act efficiently in ranges where the Si content < 3.5 wt.%. According to the poisoning mechanism, Si from the Al alloy reacts with the Ti present in the refiner to form Al-Ti-Si ternary phase and thereby degrades the grain refinement efficiency of the refiner [18]. Besides Si, Zr, and Cr are also found to have poisoning effects for these Ti-based grain refiners and may suffer from premature fading or partial refinement of α-Al grains. In turn, it will impact the layer formation of CrB_2 or ZrB_2 on TiB_2, which lower nucleant potency of TiB_2 [19]. Rare earth element-based refiners are not only expensive but also are difficult to cast as master alloys for their addition into the Al alloy melt. Similarly, Al-B refiner could significantly refine the alloy only when silicon content in the alloy is more than 4 wt.% [18, 20].

Melt thermal treatment (MTT) is a promising process to optimize the mechanical properties of Al-Si alloys. In this process, no foreign substances are added for refinement or modification. So, the chance for the formation of any complicated intermetallic phases is avoided, which might adversely affect the properties. Many previous studies have shown that this process noticeably impacts the refinement of primary Si in Al–Si alloys (Si > 12%) [21–24]. Jun Wang et al. [25] have used this process for grain refinement of A356 alloy. They had concluded a significant decrement in primary dendrite arm length (450 to 210 mm) and improvement in strength and ductility by melt thermal treatment.

✉ Ajaya Kumar Pradhan
Ajaya.meta@mnit.ac.in; 2017rmt9064@mnit.ac.in

[1] Department of Metallurgical and Materials Engineering, Malaviya National Institute of Technology Jaipur, Jaipur 302017, India

MTT has been studied only to a limited extent [25–28] and no significant investigation has been conducted that studies the effects of MTT on Al-Si alloys at different silicon contents. Hence, the goal of the current study is to comparatively analyze the effects of Al-5Ti-1B grain refiner and MTT on microstructure and mechanical properties of hypoeutectic Al–xSi alloys.

Experimental Procedure

Hypereutectic Al-15Si alloy was synthesized using commercially pure aluminum and silicon. Then, various hypoeutectic Al-Si alloys of varying Si content (0, 1, 3, 5, 7, 9 wt.%) were prepared by the addition of calculated amount of commercially pure Al to the prepared Al-15Si alloy. Calculated quantities of commercially pure Al and previously formed hypereutectic alloy (Al-15Si) were melted at 720 °C in a furnace with an electrical resistance heating furnace using a clay-graphite crucible. The melt was held for 1 hour at the set temperature for homogenization. Finally, the melt was poured into preheated (300 °C) graphite molds for casting. For grain refinement of selected alloys, 0.6 wt.% of Al-5Ti-1B was added into the melt in the furnace and was further held for 15 min. During holding, a graphite rod was used to stir the melt to prevent segregation of the nucleant particles. Finally, the melt was poured into preheated cylindrical graphite mold (ø 24 mm × 120 mm) for casting and cooling rate of solidification was approximately 10 °C/s.

For melt thermal treatment process, calculated quantities of commercially pure Al and Al–15Si alloy were melted in the same furnace at 720 °C and were held for 20 min only. Then, half of the melt, termed as high-temperature melt (HTM), was transferred to another furnace held at temperature 900 °C and the other half of the melt, termed as low-temperature melt (LTM), was transferred to a furnace held at temperature 600 °C. These HTM and LTM were held at their respective temperatures for 15 min. Then, the HTM was poured into the LTM, followed by pouring of the entire melt into a preheated mold for casting. Cover flux (45 g NaCl + 45 g KCl + 10g NaF) was used throughout the melting process to prevent oxidation and C_2Cl_6 tablet was used as a degasser.

Optical emission spectrometer was used for the chemical composition analysis of commercially pure Al, Al–15Si, and Al–Ti–1B cast specimens (Spectro Lab) listed in Table 1. Chemical composition analysis of prepared unrefined Al–xSi alloy is listed in Table 2. The prepared samples were cut perpendicular to the centreline axis and polished through standard methods for metallographic examinations. Post-polishing Keller' reagent was used as etchant (95% H_2O + 2.5% HNO_3 + 1.5% HCl + 1% HF) for microstructural examination, and for macrostructural analysis, the samples were etched with Poulton's etchant (60% HNO_3 + 30% HCl + 5% HF + 5% H_2O). The microstructure of the etched samples was examined with the help of an inverted optical microscope (Zeiss Axio vert. A1) equipped with image analysis software. The macrostructure of the samples was observed using a stereo microscope at 12X magnification. Grain size analysis was carried out on the images using ImageJ software by line intercept method. Two different samples were examined at different locations and at least 10 readings for each sample were taken for grain size measurement. Secondary dendritic arm spacing (SDAS) was also measured in each image. The reported value is the average of at least 10 readings measured on at least three images.

A universal testing machine (Model: H25KL, Tinius Olsen) operated at a strain rate of 1 mm/min was used for tensile testing. In order to ensure reproducibility, the testing was carried out on at least two different samples prepared separately under similar conditions. For tensile testing, specimens were prepared as per ASTM standard E08. Vickers

Table 1 Chemical composition of raw materials

Element	Si	Mg	Fe	Ti	Cu	Mn	Zn	V	B	Al
Pure Al	0.25	0.001	0.09	0.008	0.001	0.005	0.01	0.01	–	Bal.
Al–15Si	14.8	0.01	0.24	0.006	0.001	0.004	0.001	0.012	–	Bal.
Al–5Ti–1B	0.05	–	0.15	4.98	–	–	0.01	0.01	0.97	Bal.

Table 2 Chemical composition analysis of prepared alloys

Element	Si	Mg	Fe	Ti	Cu	Mn	Zn	V	Al
Al–0Si	0.25	0.001	0.107	0.008	0.001	0.005	0.007	0.010	Bal.
Al–1Si	1.08	0.001	0.130	0.010	0.001	0.004	0.008	0.015	Bal.
Al–3Si	2.96	0.001	0.139	0.010	0.001	0.005	0.007	0.014	Bal.
Al–5Si	4.74	0.001	0.182	0.010	0.001	0.005	0.007	0.014	Bal.
Al–7Si	7.16	0.001	0.188	0.005	0.002	0.006	0.005	0.005	Bal.
Al–9Si	8.74	0.001	0.221	0.010	0.001	0.007	0.005	0.014	Bal.

microhardness was measured at ten different positions of at least two different samples using a load of 200 g and a dwell time of 15 s. The reported results are the mean of all those measurements.

Results and Discussion

Microstructural Analysis

Effect of Si Content

Figure 1 represents macrostructure of samples with different Si contents. Grain refiner was not used for these samples. The macrostructure of pure Al (x = 0) consists of coarse and columnar α-Al dendrites (Fig. 1a). With an increase in Si content in alloy, significant changes in the grain size and shape were observed. Initially, columnar structure was observed for Al–1Si alloy similar to that of pure Al. However, at 3 wt.% of Si content, the primary α-Al grains become cellular-like shape with an average grain size of 520 µm was observed in case of the Al–3Si alloy. Further increase in Si content produces larger grains without any change in shape. Figure 2 shows the relation between grain size and growth restriction factor (GRF) in unrefined alloys. The results show that in the case of all Si-containing alloys, the grain size tends to be finer than that of the pure Al. In the case of pure Al, an average grain size was 1240 µm and the minimum value of grain size (520 µm) in the case of Al–3Si alloy. Johnsson and Backerud [29] had reported that the grain size of α-Al increases above a transition point because of the altered mechanism of dendrites growth. According to them, the Si slows down the interface movement at lower content, and at higher content, the dendrite becomes sharper and rejects Si perpendicular to the growth direction. As a result**,** grains easily grow in the growth direction and grain coarsening occurs.

This transition in grain size can also be co-related in terms of the growth restriction factor (GRF) [9]:

$$\mathrm{GRF} = C_o m(k-1) \quad (1)$$

where C_o is solute concentration, m is the slope of melt and k is the partition coefficient at the solid/liquid interface. The m(k-1) value for Ti and Si is 245.6 and 6.1, respectively [9]. The calculated values of GRF are 7.6, 19.4, 31.2, 43.1, and 54.8, respectively, for the unrefined Al–1Si, Al–3Si, Al–5Si, Al–7Si, and Al–9Si alloys, in the present case. The increase in the GRF value from 19.4 to 31.2 is responsible for the increase in grain size from 520 to 710 µm in case of the Al–3Si (transition point) and Al–5Si alloy, respectively. Research by Spittle et al. [30] had also shown the same trend and they concluded that there is a sudden decrease in grain size of α-Al at lower Si but after a critical value of GRF (20 for 3 wt.% Si as solute) the grain coarsening occurs in Al-Si alloy. Another research done by Y.C. Lee et al. [31] revealed that the grain size transition above 3 wt.% Si is due to the loss of potency of nucleants or decrease in number of activated nucleants.

Figure 3 illustrates optical images of unrefined Al-xSi alloys below and above the transition point (Al-3Si). The microstructure consists of coarse α-Al dendrites (bright

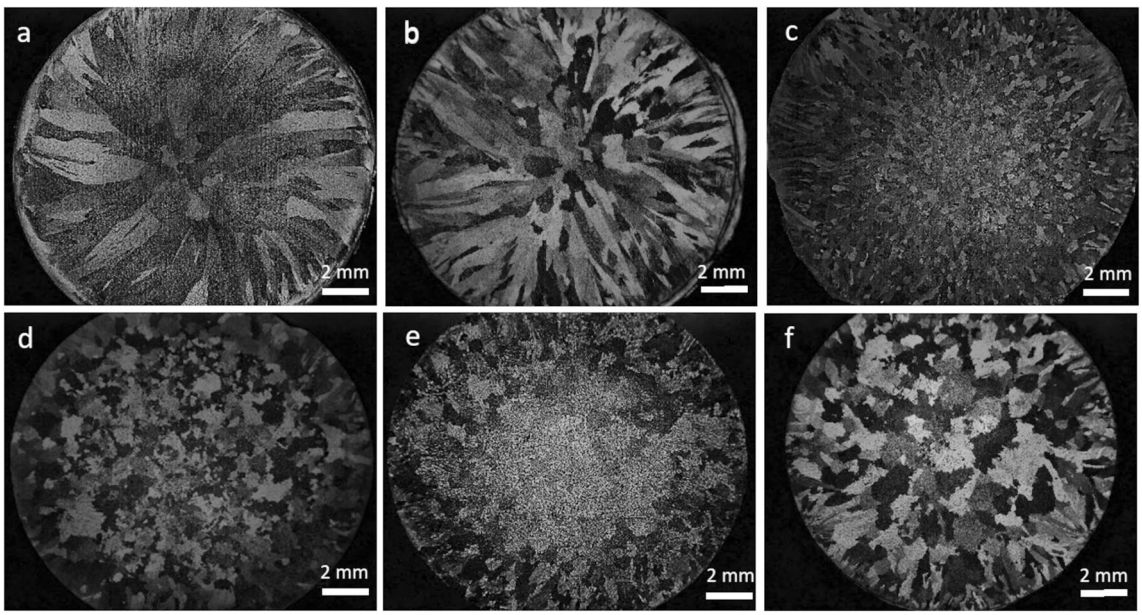

Fig. 1 Macrostructure of unrefined Al-xSi alloy (**a**) x = 0, (**b**) x = 1, (**c**) x = 3, (**d**) x = 5, (**e**) x = 7, and (**f**) x = 9

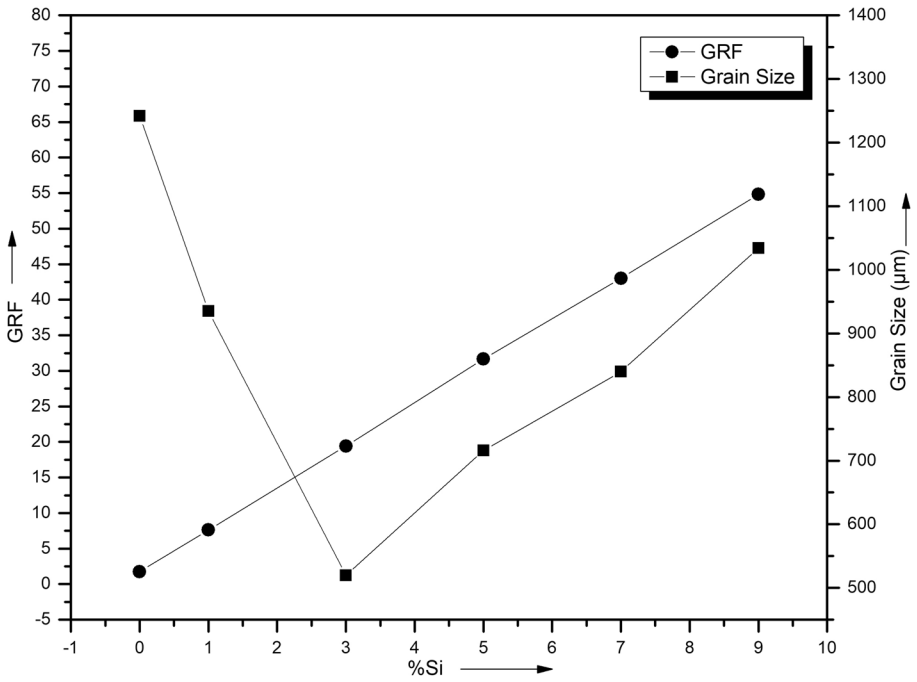

Fig. 2 Relation between grain size and GRF with silicon content of unrefined alloys

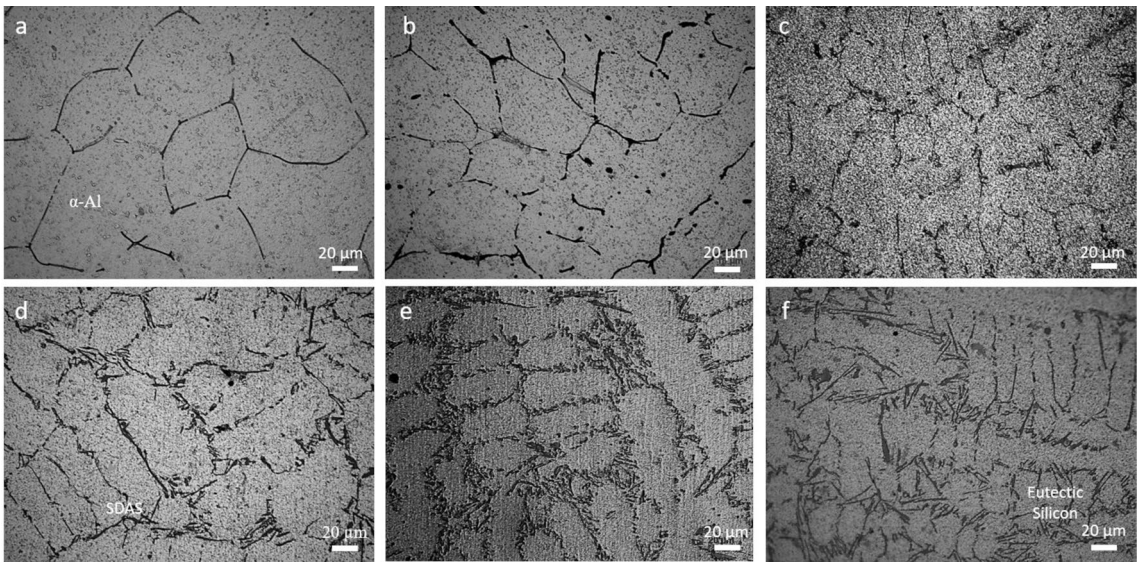

Fig. 3 Optical microstructure of unrefined hypoeutectic Al–xSi alloy (**a**) x = 0, (**b**) x = 1, (**c**) x = 3, (**d**) x = 5, (**e**) x = 7, and (**f**) x = 9

region) and Al-Si eutectic (black acicular structure) at inter-dendritic regions. It may further be observed that the shape of α–Al grains changes from cellular structure to dendritic structure after the transition point (3 wt.% of Si) [32]. Below 1.65 wt.% (that is the solubility limit of Si in Al [1]) Si content in the alloy (i.e., pure Al and Al-1Si alloy in the present case), the microstructure only consists of cellular α-Al matrix. Similar changes in the shape of α-Al grains were observed in the case of refined and MTT-processed alloys with Si content.

Figure 4 represents macrostructures of specimens of Al–1Si alloy (Fig. 4a, b, and c) and Al-5Si alloy (Fig. 4d, e, and f) without any addition or treatment with 0.6 wt.% grain refiner addition and melt thermal treatment, respectively. Results suggest maximum reduction in grain size occurs in grain refined Al-Si alloy and MTT-processed Al-5Si alloy as against to unrefined alloy. Al-1Si alloy and

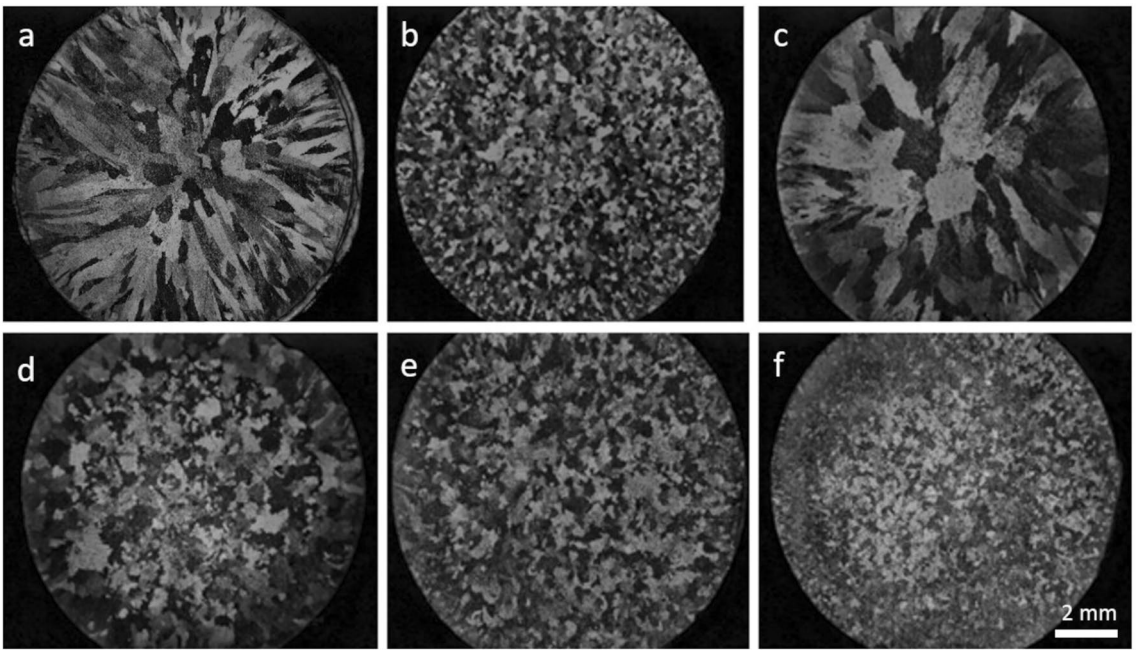

Fig. 4 Macrostructure Al–1Si and Al–5Si alloy: (**a** and **d**) unrefined, (**b** and **e**) with 0.6% GR, and (**c** and **f**) after MTT, respectively

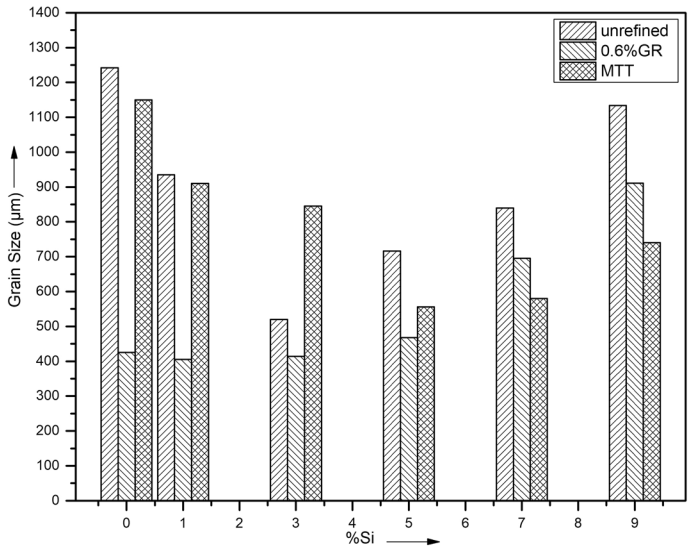

Fig. 5 Variation in grain size of unrefined, chemical-refined, and MTT-treated sample

Al-5Si alloy are representative macrostructures of alloys below and above the transition point, respectively. Figure 5 shows correlation of average grain size with different silicon contents. Grain size of the alloys treated with Al-5Ti-1B reduces in every case compared to the unrefined alloy. However, the effectiveness of grain refinement is only up to the transition point (Si = 3%), and afterward, the effectiveness of the refiner reduces. The grain size of refined Al-1Si alloy decreased from 935 to 405 μm (~ 56% reduction), whereas that of refined Al-5Si alloy decreased from 716 to 468 μm (~ 34% reduction). The maximum refinement of grains is found in the case of pure Al (~ 65% reduction) and the minimum refinement for Al-3Si alloy (~ 20% reduction).

Figure 5 also shows that for the unrefined alloy, the changes in grain size below the transition point are higher than above the transition point. In the case of the refined alloy, the change in grain size below the transition point is less significant. However, above the transition point, the change in grain size is comparable to that of the unrefined alloy. It signifies the increase in grain size because silicon is more dominant than decrement in grain size because of grain refiner above the transition point. The reason behind the reduction in the effectiveness of the grain refiner is the

poisoning of Ti by Si in the melt. According to this effect, nucleation of silicide on the Ti-containing nucleant particles ($AlTi_3$) leads to poor potency of nucleant particles. Besides, Si reduces the solubility of Ti in α-Al matrix by forming $TiSi_2$ [2, 16, 33]. These two effects result in reduced surface area for nucleation and decreased value of GRF, and hence reduced the size of the undercooled zone in which the nuclei become activated. Easton et al. [34] had concluded that the lower value of partition coefficient (k) of Ti in refined alloy is the reason of lowering of grain refining effectiveness of Al–5Ti–1B in aluminum silicon alloys (Si > 5%).

In the case of MTT-treated alloys, grain size of Al-Si alloy below the transition point is comparable to that of unrefined alloy. However, above the transition point (Si > 3%), the grain sizes were smaller compared to both unrefined alloys and refined alloys. The grain size reduction in MTT-treated alloys is approx. 7 and 22%, respectively, in case of Al-1Si alloy and Al-5Si alloy, compared to the unrefined alloys. The maximum reduction observed is 34.7% and that is in the case of MTT-treated Al-9Si alloy compared to unrefined Al-9Si alloy. The reason behind this is the existence of lots of atomic clusters such as Al-Al, Al-Si, and Si-Si in the Al-Si melt [35]. In case of high-temperature melt (HTM), Al-Al and Si-Si atomic clusters dissipate heat leading to the formation of Al-Si clusters. This change in liquid structure at high temperature tends to decrease the size and hence increase the number of these clusters [36, 37]. Thus, number of nuclei for solidification of α-Al increase and grain size decreases. However, the number of Si-Si atomic clusters was less in low Si content alloys compared to high silicon content alloys. That is why favorable impact of MTT process on grain size of α-Al is lesser in the case of low silicon content alloys.

The mechanism of MTT process for hypoeutectic Al–Si alloy is proposed by Wang [25] and Peng [26]. According to this mechanism, when the melt temperature is close to melting point of alloy, a number of solid-like clusters get formed in the melt and such structures are known as micro-homogenous structure. MTT technique can change these micro-inhomogeneous structures into nano-size homogenous structure. When melt temperature reaches up to 890–950 °C, larger sized atomic clusters convert into smaller nano-size atomic clusters and the melt gets a uniform distribution of these clusters [38]. These nano-sized homogenous structures can be retained at pouring temperature by mixing of the chilled alloy melt or low-temperature alloy melt of the same composition. These mixing bring many small and uniformly distributed solid-like atomic clusters in the melt that tend to act as crystal nucleus of α-Al phases. Also, low-temperature melt has semisolid content, which leads to free secondary dendritic arms when mixed with high-temperature melt. These free secondary dendritic arms also act as heterogeneous nucleation sites for α-Al.

Figure 6 shows representative optical microstructure of Al–9Si alloy prepared under different casting conditions. The results of Fig. 6a, c, e indicate that MTT process reduces the average length of primary dendritic arms from 690 ± 30 µm (unrefined alloy) to 345 ± 15 µm. This is by the breaking primary dendrite arms after intermixing of melts [25]. These results are also reflected in the research of Wang et al. [25], who have shown that the primary dendritic length decreased from 650 to 410 µm by melt thermal treatment in A356 alloy. Figure 6b, d, f indicates that MTT process also causes partial refinement of eutectic Si particles by which the coarse silicon particles are broken up into smaller pieces and this has neither been observed in unrefined alloys nor in refined alloys. However, the morphology of eutectic Si remains acicular in each of the alloys. The average length of eutectic Si in Al–9Si alloys (representative microstructure) is 29.85, 32.51 and 17.28 µm, respectively, in unrefined, refined, and MTT alloys.

Effect of SDAS

The influence of different contents of silicon on SDAS is shown in Fig. 7. SDAS decreases as the silicon content increases under similar cooling conditions. However, after 5 wt.% of Si, the slope of the curve was observed to be less stepper. Marko Grzincic explains the reason in one of his research [39]. According to him, the gaps in-between α-aluminum dendrite arms increase in order to facilitate the growing quantities of solute elements (i.e., Si in the present case).

Figure 8 represents microstructures of unrefined Al–Si alloys with various silicon contents. It was observed that the dendritic structure is more compact at 3 wt.% of Si and it became more visible at 9 wt.% of Si. This happens because of the growing eutectic phase fraction in the region of inter-dendrite, which reduces the average value of SDAS from 31.6 µm in case of 3 wt.% Si to 25.1 µm in case of 5 wt.% Si and 18.5 µm in case of 9 wt.% Si. There is no noticeable alteration in SDAS in each of the hypoeutectic Al–Si alloys after the addition of grain refiner and after MTT process. The changes in SDAS of Al–9Si alloys are shown in Fig. 6(a, c, e). The calculated average values of SDAS are 18.5, 17.36 and 17.79 µm in case of unrefined, refined, and MTT-treated Al–9Si alloys, respectively.

Mechanical Properties

Figure 9 displays the variations in ultimate tensile strength (UTS), Vickers hardness (VHN), and elongation of Al–xSi alloys prepared under different casting conditions. In the unrefined alloy, strength and hardness increase with the increasing Si content. The maximum value of UTS and VHN was observed in the case of Al–9Si alloy. This indicates role

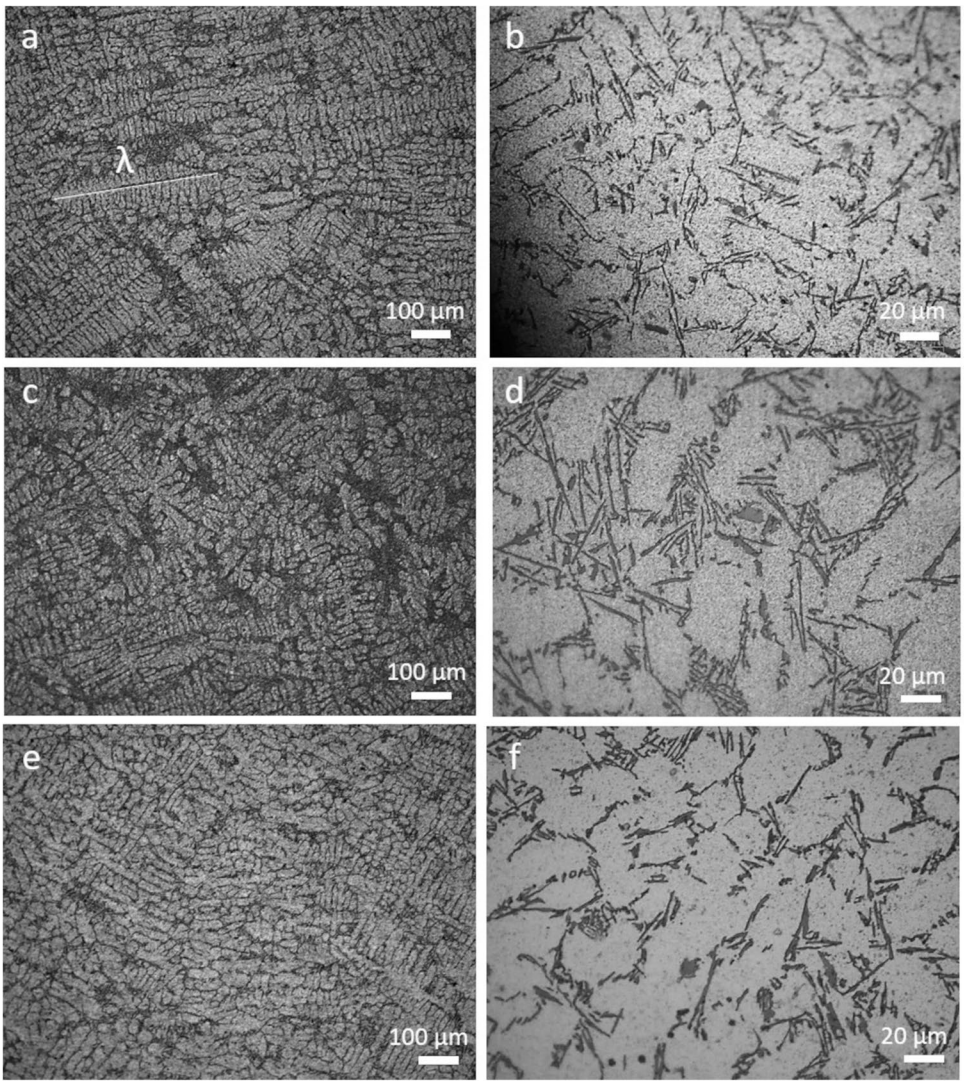

Fig. 6 Optical microstructure of Al-9Si alloy: (**a**, **b**) unrefined, (**c**, **d**) grain refined, and (**e**, **f**) MTT

of Si is more dominative to increase these properties than the grain refinement and MTT process. This observation is based on solid solution strengthening and dispersion strengthening provided by Si atom and its pure phase and the increasing content of eutectic Al–Si phase. The maximum value of UTS and VHN obtained in the case of the unrefined Al–9Si alloy are 175 MPa (73.9% increment compared to Al–1Si) and 54.3 (64.1% increment compared to Al–1Si), respectively. However, the ductility of the samples also decreased continuously with the increasing Si content. As an increase in silicon content, the volume fraction of eutectic phase (which is harder than compare to α-Al matrix) increases, leading to an increment in strength and hardness. In each of the refined alloys, the UTS, VHN, and elongation were higher than the corresponding unrefined alloy. However, the change in tensile strength and hardness below the transition point (Si = 3%) for grain-refined alloys was significant than above it. It is because of the noticeably higher variation in the grain size above the transition point by the introduction of the grain refiner.

The quantitative values obtained in the case of Al-1Si alloy and Al-5Si alloy were representatively presented below. The UTS, VHN, and elongation were increased by 21.35, 12.5 and 34.3%, respectively, because of grain refinement in case of the Al-1Si alloy. However, they only increased by 9.48, 4.32 and 22.9%, respectively, in the case of the Al-5Si alloy.

The results also show that after MTT process, UTS and hardness increase significantly below the transition point than above it (Al–3Si) compared to that of the unrefined and refined alloy. The UTS and VHN of MTT-treated Al–1Si increased by 26.5 and 27.4%, respectively, compared to that of the unrefined Al-1Si. The improvement in these properties was observed to be limited beyond the transition points. The UTS and VHN of MTT-treated

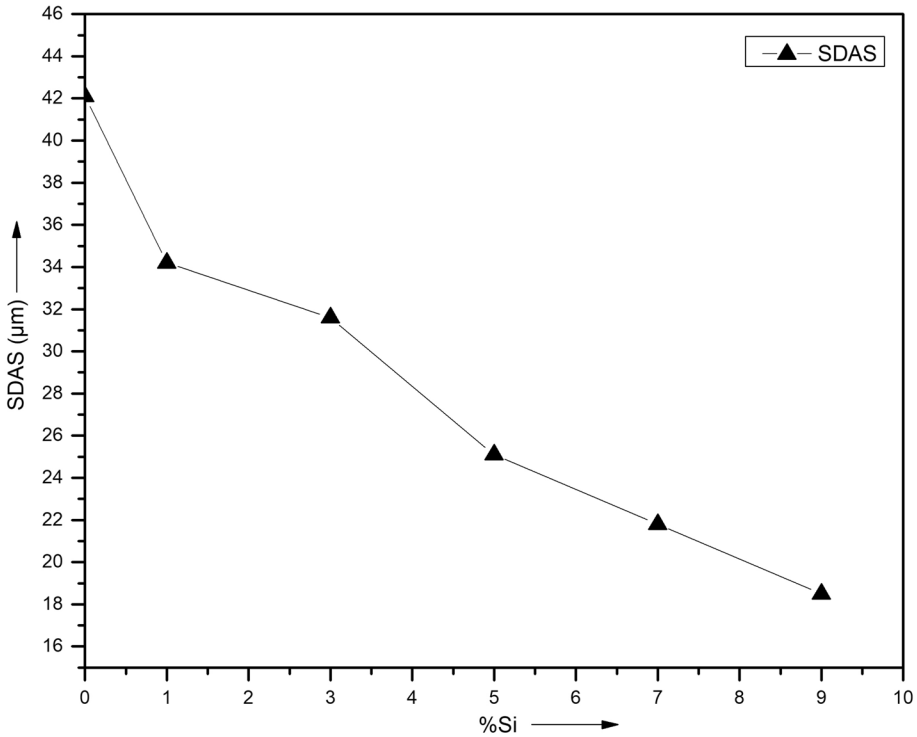

Fig. 7 Effect of Si content on SDAS

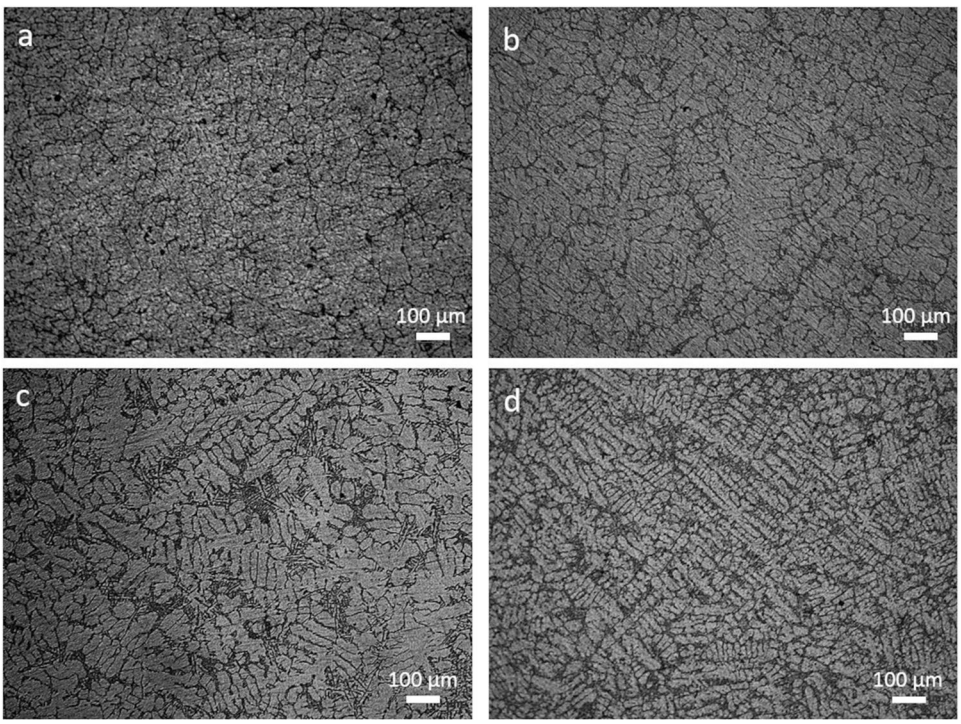

Fig. 8 Optical microstructure of unrefined Al–xSi alloy (**a**) x = 3, (**b** x = 5, and (**c**) x = 9

Al–5Si increased only by 5.3 and 5.2%, respectively, compared to that of the unrefined Al–5Si.

Conclusions

Following are the conclusions that came out of the presented study.

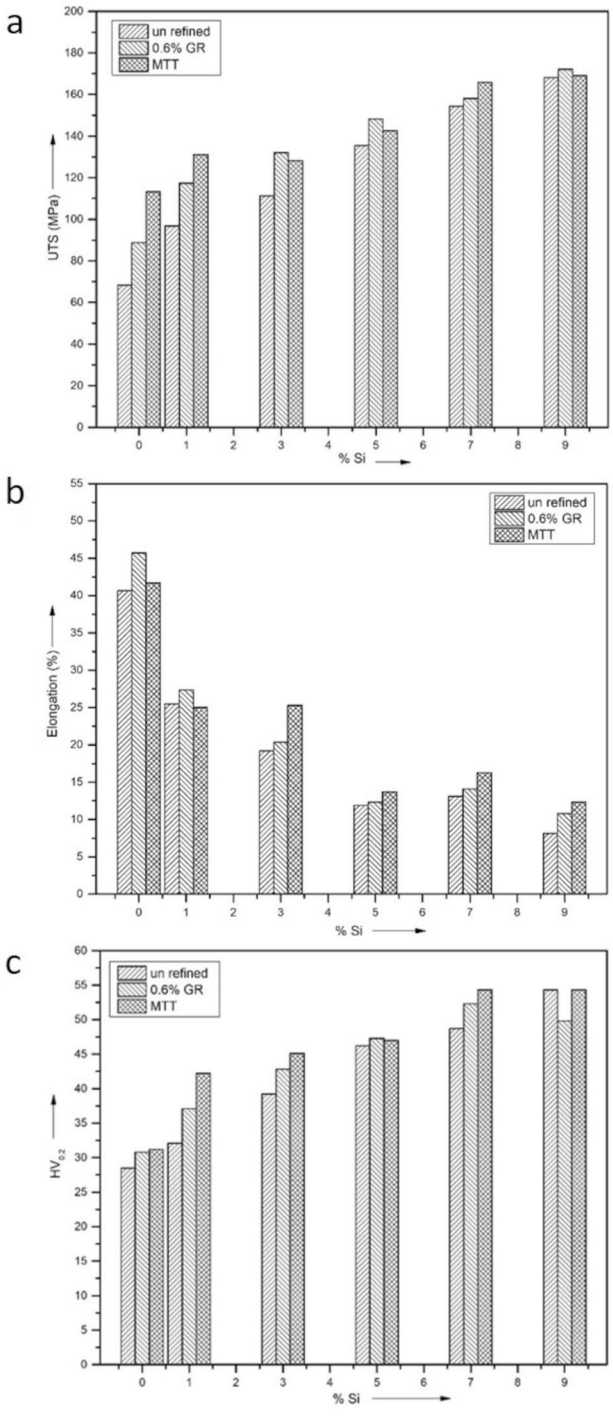

Fig. 9 Variations in ultimate tensile strength (UTS), Vickers hardness (VHN), and elongation of Al–xSi alloy prepared under different casting conditions

- The smallest grains get produced at Al-3 wt.% Si alloy in unrefined, refined, and MTT-processed alloys.
- Addition of grain refiner causes significant reduction in grain below the transition point. Beyond this, the role of Si is more dominating than poisoning of Ti by Si for decreasing grain size.
- In the case of MTT-treated alloys, the grain size of Al-Si alloy below the transition point is comparable to that of unrefined alloy. However, above the transition point (Si > 3%), the grain sizes were smaller compared to both unrefined alloys and refined alloys.
- After MTT process, UTS and hardness increase significantly only below the transition point compared to that of the unrefined and refined alloys.

References

1. J.R. Davis, *ASM Speciality Handbook: Aluminum and Aluminum Alloys* (ASM International, Ohio, 1993)
2. Y. Li, B. Hu, B. Liu, A. Nie, Q. Gu, J. Wang, Q. Li, Insight into Si poisoning on grain refinement of Al-Si/Al–5Ti–B system. Acta. Mater. **187**, 51–65 (2020)
3. S.G. Shabestari, R. Gholizadeh, Investigation on the microstructure and mechanical properties of new Al−Si piston alloys. J. Adv. Mate. Res. **445**, 289–294 (2012)
4. M. Amne-Elahi, S.G. Shabestari, Effect of various melt and heat treatment conditions on impact toughness of A356 aluminum alloy. Trans. Nonferrous. Met. Soc. China. **26**, 956–965 (2016)
5. P.T. Li, S.D. Liu, L.L. Zhang, Grain refinement of A356 alloy by Al–Ti–B–C master alloy and its effect on mechanical properties. Mater. Des. **47**, 522–528 (2013)
6. Z. Fan, F. Gao, Y. Wang, H. Men, L. Zhou, Effect of solutes on grain refinement. Prog. Mater. Sci. (2022). https://doi.org/10.1016/j.pmatsci.2021.100809
7. H. Liao, M. Zhang, Q. Wu, Refinement of eutectic grains by combined addition of strontium and boron in near eutectic Al-Si alloys. Scr. Mater. **57**, 1121–1124 (2007)
8. S.M. Jigajinni, K. Venkateswarlu, S.A. Kori, Computer aided cooling curve analysis for Al–5Si and Al–11Si alloys. Int. J. Eng. Sci. Tech. **3**(6), 257–272 (2011)
9. K.T. Kashyap, T. Chandrashekar, Effects and mechanisms of grain refinement in aluminium alloys. Bull. Mater. Sci. **24**(4), 345–353 (2001)
10. D.G. Mallapur, S.A. Kori, Studies on the influence of grain refining and modification on microstructure and mechanical properties of forged A356 alloy. Mater. Sci. Eng. A. **528**, 4747–4752 (2011)
11. T. Wang, H. Fu, Z. Chen, A novel fading-resistant Al−3Ti−3B grain refiner for Al−Si alloys. J. Alloys. Compd. **511**(1), 45–49 (2012)
12. H. Li, T. Sritharan, Y.M. Lam, N.Y. Leng, Effects of processing parameters on the performance of Al grain refinement master alloys Al–Ti and Al–B in small ingots. J. Mater. Process. Technol. **66**, 253–257 (1997)
13. S.A. Kori, B.S. Murty, M. Chakraborty, Influence of silicon and magnesium on grain refinement in aluminium alloys. Mater. Sci. Technol. **15**, 986–992 (1999)
14. P. Tang, W.F. Li, K. Wang, Effect of Al–Ti–C master alloy addition on microstructures and mechanical properties of cast eutectic Al–Si–Fe–Cu alloy. Mater. Design. **115**, 147–157 (2017)
15. X.J.C. Wang, C. Xu, A. Muhammad, Effects of Al–Ti–B–RE grain refiner on microstructure and mechanical properties of Al-7.0Si-0.55Mg alloy. Trans. Nonferr. Metal. Soc. **24**, 2044–2050 (2014)

16. D. Qiu, J.A. Taylor, M.X. Zhang, P.M. Kelly, A mechanism for the poisoning effect of silicon on the grain refinement of Al–Si alloys. Acta. Mater. **55**, 1447–1456 (2007)
17. X. Dong, J. Shouxun, Si poisoning and promotion on the microstructure and mechanical properties of Al–Si–Mg cast alloys. J. Mater. Sci. **53**, 7778–7792 (2018)
18. Y. Birol, Effect of silicon content in grain refining hypoeutectic Al–Si foundry alloys with boron and titanium additions. Mater. Sci. Technol. **28**, 385–389 (2012)
19. J.A. Spittle, S. Sadli, The influence of zirconium and chromium on the grain-refining efficiency of Al–Ti–B inoculants. Cast Metals. **7**(4), 247–253 (1995)
20. H.D. Alamidari, D. Dube, P. Tessier, Behavior of boron in molten aluminum and its grain refinement mechanism. Metall. Mater. Tran. A. **44A**, 388–394 (2013)
21. Q. Wang, H.S. Geng, S. Zhang, Effects of melt thermal- rate treatment on fe-containing phases in hypereutectic Al–Si alloy. Metall. Mater. Tran. A. **45**, 1621–1630 (2014)
22. B. Xiufang, W. Weimin, Thermal-rate treatment and structure transformation of Al–13 Wt.% Si alloy melt. Mater. lett. **44**, 54–58 (2000)
23. Q. Wang, G. Haoran, Study of melt thermal-rate treatment and low-temperature pouring on Al-study of melt thermal-rate treatment and low-temperature pouring on Al–15% Si Alloy. J. Mater. **65**, 958–966 (2006)
24. T. Ohmi, M. Kudoh, Control of primary silicon crystal size of semi-solid hypereutectic Al–Si alloy by slurry-melt mixing process. J. Jpn. Inst. Met. **58**, 1311–1317 (1994)
25. J. Wang, S. He, B. Sun, Effects of melt thermal treatment on hypoeutectic Al–Si alloys. Mater. Sci. Eng. A. **338**, 101–107 (2002)
26. P. Jia, J. Zhang, H. Xun, X. Teng, M. Zuo, Z. Gao, C. Yang, D. Zhao, Grain refining effects of the melt thermal-rate treatment and Al-Ti-B-Y refiner in as-cast Al-9Si-0.5Mg alloy. Mater. Res. Express. **5**(6), 066520 (2018). https://doi.org/10.1088/2053-1591/aac994
27. S.A. Al Kahtani, H.W. Doty, F.H. Samuel, Combined effect of melt thermal treatment and solution heat treatment on eutectic Si particles in cast Al-Si alloys. Int. J. Cast Met. Res. **27**, 38–47 (2014)
28. P. Ashtari, G. Birsan, A. Khalaf, S. Shankar, Controlled diffusion solidification of 2024, 6082 and 7075 Al alloys via tilt-pour casting process. Inter. Metal cast. **5**, 43–64 (2011)
29. J. Mats, L. Backerud, G.K. Sigworth, Study of the mechanism of grain refinement of aluminum after additions of Ti- and B-containing master alloys. Metall. Tran. A. **24**, 481–491 (1993)
30. J.A. Spittle, S.B. Sadli, Effect of alloy variables on grain refinement of binary Al alloys with Al-Ti-B. Mater. Sci. Technol. **11**, 533–537 (1995)
31. Y.C. Lee, A.K. Dahle, D.H. Stjohn, the effect of grain refinement and silicon content on grain formation in hypoeutectic Al – Si alloys. Mater. Sci. Eng. A. **259**, 43–52 (1999)
32. P.S. Mohanty, J.E. Gruzleski, Grain refinement mechanisms of hypoeutectic Al–Si alloys. Acta. Metall. Mater. **44**, 3749–3760 (1996)
33. V.E. Bazhenov, M.A. Magura, Effects of Si and Cu contents on grain size of Al–Si–Cu alloys. Mater. Sci. Technol. (2018). https://doi.org/10.1080/02670836.2018.1425237
34. M. Easton, S. David, (1996) Grain Refinement of Aluminum Alloys : Part I . The Nucleant and Solute Paradigms–A Review of the Literature. 30, 1613–23
35. Z.W. Chen, W.Q. Jie, R.J. Zhang, Superheat treatment of Al–7Si–0.55 Mg alloy melt. Mater. Lett. **59**, 2183–2185 (2005)
36. I. Shtablavyi, S. Mudry, V. Mykhaylyuk, J. Rybicki, The structure of Al–Cu and Al–Si eutectic melts. J. Non-Cryst. Solids. **354**, 4469–4474 (2008)
37. T.F. Banamove, Superheating and refining. M. Mech. **255**, 112–123 (1965)
38. X.F. Zhang, X. Yang, F.Q. Zu, Q.L. Chen, H.C. Cai, On Optimizing of solidification structure of Al-Si alloys by using melt mixing treatment process. Spec. Cast. Nonferrous Alloys. **35**, 482–485 (2015)
39. M.B. Djurdjevic, M.A. Grzincic, The effect of major alloying elements on the size of secondary dendrite arm spacing in the As-cast Al-Si-Cu alloys. Arch. Foundry. Eng. **2**(1), 19–24 (2012)